Published in final edited form as:
Mol Cancer Ther. 2014 December ; 13(12): 2968–2977. doi:10.1158/1535-7163.MCT-14-0354.

Radiation protection of the gastrointestinal tract and growth inhibition of prostate cancer xenografts by a single compound

Vitali Alexeev[1], **Elizabeth Lash**[1], **April Aguillard**[1], **Laura Corsini**[1], **Avi Bitterman**[1], **Keith Ward**[2], **Adam P. Dicker**[3], **Alban Linnenbach**[1], and **Ulrich Rodeck**[1,3]

[1]Department of Dermatology, Thomas Jefferson University, Philadelphia, PA 19107, USA

[2]REATA Pharmaceuticals, Irving, TX 75063

[3]Department of Radiation Oncology, Thomas Jefferson University, Philadelphia, PA 19107, USA

Abstract

Normal tissue toxicity markedly reduces the therapeutic index of genotoxic anti-cancer agents including ionizing radiation. Countermeasures against tissue damage caused by radiation are limited by their potential to also protect malignant cells and tissues. Here we tested a panel of signal transduction modifiers for selective radioprotection of normal but not tumor tissues. These included three inhibitors of GSK3 (LiCl, SB216763 and SB415286) and two inhibitors of NF-κB (ethyl pyruvate and RTA 408). Among these, the thiol reactive triterpenoid RTA 408 emerged as a robust and effective protector of multiple organ systems (gastrointestinal, skin and hemopoietic) against lethal doses of radiation. RTA 408 preserved survival and proliferation of crypt cells in lethally irradiated small intestines while reducing apoptosis incidence in crypts and villi. In contrast, RTA 408 uniformly inhibited growth of established CWR-22Rv1, LNCaP/C4-2B, PC3 and DU145 xenografts either alone or combined with radiation. Anti-tumor effects in vivo were associated with reduced proliferation and intratumoral apoptosis and with inhibition of NF-κB-dependent transcription in PC3 cells. Selective protection of normal tissue compartments by RTA 408 critically depended on tissue context and could not be replicated in vitro. Collectively, these data highlight the potential of RTA 408 as a cytoprotective agent that may be safely used in chemoradiation approaches.

Keywords

Thiol reactive compound; radiation protection; tumor growth inhibition

Introduction

Radiation therapy is the most common therapeutic modality across a wide range of malignant diseases including prostate cancer. However, the delivery of curative radiation doses is hampered by acute or chronic ‘collateral damage’ affecting normal tissues. When

Corresponding author:. Ulrich Rodeck, Thomas Jefferson University, 233 S 10th Street; BLSB409, Philadelphia, PA 19130, USA, Tel/Fax: 215-503-5622 ulrich.rodeck@jefferson.edu.

Conflict of interest: Keith Ward is employed by and has a financial interest in REATA Pharmaceuticals, Inc.

treating tumors in the abdominal cavity, toxicity to the intestine and the bladder are often dose-limiting (1). Highly targeted methods to deliver radiation specifically to disease sites alleviate radiation toxicity, yet 40% – 50% of patients with locally advanced prostate cancers recur locally following treatment (2). Hence protection of normal tissue will be a critical element of future dose escalation trials in patients with locally advanced prostate cancer. Existing radiation protectors including amifostine (3) are of limited utility in protecting the small and large intestines against radiation effects.

Inflammation is a key element of the radiation response of normal and tumor tissues and is commonly associated with increased activity of nuclear factor-kappaB (NF-κB) (4, 5). Previously we demonstrated that several inhibitors of canonical NF-κB activation improved survival of lethally irradiated zebrafish embryos and preserved gastrointestinal morphology and function (6). Inhibitors of glycogen synthase kinase (GSK)3 similarly protect normal tissues including the gastrointestinal tract (7, 8). While the role of GSK3β in cell stress responses is complex (for review (9)), it has been implicated in modifying NF-κB-dependent transcription of genes encoding proinflammatory proteins (10, 11).

Here we performed a side-by-side comparison of radioprotective properties of five compounds targeting either GSK3 and/or NF-κB with a focus on the gastrointestinal tract. We report that the triterpenoid RTA 408 provides robust radiation protection to the GI system of mice and markedly improves overall survival of lethally irradiated mice. Importantly, normal tissue protection by RTA 408 is contrasted by inhibition of human prostate cancer xenograft growth in mice.

Materials and Methods

Materials and cells

Compounds were obtained from the following sources: Ethyl pyruvate and lithium chloride (Sigma-Aldrich), SB216763 and SB416583 (Tocris Bioscience), amifostine (Medimmune), and 2-cyano-3,12- dioxooleana-1,9(11)-dien-28-oic acid (CDDO) derivative RTA 408 (REATA Pharmaceuticals). Prostate cancer cells (PC3, LNCaP/C4-2B, DU145 and CWR-22Rv1) were originally obtained from ATCC or Dr. Thomas Pretlow (Case Western Reserve University) and generously provided by Dr. Marja Nevalainen (Thomas Jefferson University) and immortalized NHPrE-1 and BHPrE-1 prostate epithelial cells were a gift from Dr. Simon Hayward (Vanderbilt University Medical Center). Normal primary prostate epithelial cells (PrEC) were from Lonza (Allendale, NJ). The prostate cancer cell lines were authenticated on a regular basis by monitoring cell morphology, androgen-responsiveness and the expression of cell lines specific markers. Normal primary epidermal keratinocyte cultures were established using standard protocols. Cells were routinely tested for mycoplasma contamination using MycoSensor PCR assay kit (Stratagene). Tumor cells were grown in RPMI1640 supplemented with 10% FBS (Corning Cellgro). Normal and immortalized prostate epithelial cells and primary keratinocytes were grown in specialty media (Lonza). For in vivo imaging, PC3 prostate carcinoma cells were stably transfected with reporter plasmids (pGL4.51[luc2/CMV/Neo] and pNL3.2.NF-κB-RE[NlucP/NF-κB-RE/Hygro], Promega) encoding firefly luciferase (FLuc) and NanoLuc® luciferase,

respectively and luciferase reporter activity tested using reporter-specific in vitro assays (Promega).

Toxicity studies in mice

C57Bl/6 mice (6–8 weeks old) were from Charles River Laboratories. Mice were kept in pathogen-free conditions and handled in accordance with the requirements of the Guideline for Animal Experiments and after approval of the experimental protocols by the Institutional Animal Care and Use Committee of Thomas Jefferson University. Ionizing radiation (IR) was administered at doses ranging from 5 to 30 Gy using a 250-kVp X-ray machine (PanTak, East Haven, CT) with 50-cm source-to-skin distance and a 2-mm copper filter. The dose rate was approximately 1.4 Gy/min. Drugs were uniformly administered by i.p. injection for up to 2 days prior to IR treatment, and on days 1, 2, and 3 post-IR treatment as indicated. For comparison of RTA 408 and amifostine, mice received one dose (17.5 mg/kg) of RTA 408 24 h prior IR (whole body, 9 Gy), one dose 1 hr prior to IR, and 2 additional doses 24 and 48 h after IR; amifostine was injected once (250 mg/kg) 15 min prior to IR. All injections were done i.p. Animals were euthanized at the end of the observation period, or when weight loss reached or exceeded 20% of the initial weight, or if they showed signs of severe morbidity (lethargy, hunched posture and/or shivering or severe diarrhea). Kaplan-Meier survival curves were compared by using the Log-rank (Mantel-Cox) test.

Growth inhibition of prostate cancer xenografts

Prostate carcinoma cells were inoculated by subcutaneous injection (5×10^6 per mouse) into the lower abdominal skin of male *Foxn1nu* (nude) mice (6–8 weeks old; Charles River Laboratories). Tumor progression was monitored by caliper measurements and by *in vivo* live imaging (see below). Xenografts were allowed to grow for 2–3 weeks prior to treatment. RTA 408 (17.5 mg/kg) or vehicle control (DMSO) were administered intrperitoneally three times per week until the end of the observation periods. To assess effects of the combination of RTA 408 and IR, radiation (5 Gy) was administered at different time points as indicated. Tumor volumes were calculated by multiplying the two longest planar axes measured by the depth of the tumor (as determined by caliper measurements). Mixed effects regression models were used to determine statistical significance of tumor growth data over time.

In situ imaging of xenografts and image analysis

For firefly luciferase-based *in vivo* live imaging, mice were injected i.p. with 200 μl D-luciferin in PBS (15 mg/ml) per 20 g of mouse body weight 15 minutes prior to imaging, and imaged using an IVIS In Vivo Imaging System (Caliper Life Sciences). For in vivo imaging of the NanoLuc® luciferase under the control of the NF-κB response element, 100 μl of the NanoGlo® substrate (10 μg) (Promega, Madison, WI) were injected via tail vein. Image analysis and quantitation was done using Living image 4.2 software (Caliper LifeSciences). Luciferase-positive areas on individual images were selected as Regions of Interest (ROI) with a 14% threshold. Planar spectral images were automatically analyzed by the software. Total counts for all pixels inside the ROI were recorded. At least 3 animals from each experimental group were used for each time point.

Histology, immunohistochemistry and in situ apoptosis detection

For histological, immunofluorescent and direct fluorescent analyses, tissue samples (eg. small intestines, tumors) were embedded in the OCT compound (Tissue-Tek), and cryo-sectioned (7 μm). Hematoxylin and Eosin staining was done on ethanol/acetic acid fixed slides. Apoptosis incidence was determined by terminal deoxynucleotidyl transferase dUTP nick end labeling (TUNEL) using the *In Situ* Cell Death Detection Kit (Roche Applied Science) and 4',6-diamidino-2-phenylindole (DAPI) counterstain. Quantitative analysis was done using ImagePro software (Media Cybernetics, Rockville, MD) on at least 6 different and independent microscopic fields for each treatment condition. Indirect immunofluorescence was performed by incubation with primary antibodies for cleaved PARP (Asp214) Human Specific (Cell Signaling), M30CytoDEATH (Roche Applied Science), or Ki-67 (abcam) for 1 h at room temperature or overnight at 4°C followed by secondary antibodies labeled with either Alexafluor^{488} or Alexafluor^{594} (BD Biosciences). Sections were counterstained with DAPI and slides were mounted using anti-fade Fluorosafe reagent (Calbiochem).

In vitro cell growth and viability assays

Cells were seeded in 96-well plates at 15,000 cells/well; after 24 h, RTA 408 or vehicle were added in triplicate. After 72 h, attached cells were fixed with 70% ethanol, stained with crystal violet solution (0.2% crystal violet in 2% ethanol), and quantitated by measuring absorbance (OD_{A595}). Metabolic activity was determined after 72 h by addition of WST-1 reagent (Roche; 10 μL per 100 μL supernatant) for at least 3 hr at 37° C, followed by measuring absorbance at OD_{A450} with a reference of OD_{A650} and using wells containing media without cells for background subtraction. Statistical differences betweeen treatment groups were determined using one-way ANOVA with Tukey's post-test correction (GraphPad Prism).

Immunoblot analyses

Prostate carcinoma cell lines were treated for 24 h with RTA 408 or vehicle at the concentrations indicated. Immunoblots were reacted with (a) PARP-1 primary antibody (C2-10) (Santa Cruz Biotechnology, Dallas, TX) and IRDye 800CW goat anti-mouse IgG1-specific secondary antibody; (b) Cleaved Caspase-3 (Asp175) (5A1E) primary antibody (Cell Signaling) and IRDye 800CW Donkey anti-Rabbit IgG (H + L) secondary antibody; (c) Cleaved Caspase-8 (Asp384) (11G10) primary antibody (Cell Signaling) and IRDye 800CW goat anti-mouse IgG1-specific secondary antibody, or (d) M30CytoDEATH primary antibody (Roche Applied Science) and IRDye 800CW Goat Anti-Mouse IgG2b specific secondary antibody; all secondary antibodies were from LICOR. Filters were analyzed on a LICOR Odyssey imaging system.

Colony formation assays

Cells were seeded at clonogenic densities in T-25 flasks and treated with RTA 408 at various concentrations or DMSO, at 24 and 1 h prior to radiation exposure. IR was administered at 0, 2, 4, 6, and 8 Gy. All treatments were performed in biological triplicate. Following IR, flasks were incubated for 2 weeks. Colonies were identified by crystal violet

staining; those containing ≥50 cells were counted. The data were fit to a linear quadratic model for cell survival by using GraphPad Prism software and the equation Y=exp(−a*x −b*x^2) (12). Statistically significant differences between drug and control curves were determined by using two-way ANOVA.

Results and Discussion

Inhibitors of canonical NF-κB activation and of GSK3 improve survival of lethally irradiated mice

We performed a side-by-side comparison of several NF-κB and GSK3 inhibitors on mice challenged with a lethal whole body radiation dose (8 Gy) (Figure 1). All of the compounds reportedly protect against or mitigate radiation injury in different experimental settings either in vitro or in vivo. They included two inhibitors of canonical NF-κB signaling (ethyl pyruvate (13)) and RTA 408 (14))(Figure 1a), and three GSK3 inhibitors including lithium chloride (LiCl) (8), SB415286 (8), and SB216763 (8) (Figure 1b,c). Ethyl pyruvate interferes with NF-κBp65 signaling by covalently modifying a reactive cysteine residue (Cys36) of the NF-κBp65 subunit (15). RTA 408 is a variant of the triterpenoid CDDO that reversibly and covalently modifies reactive cysteine residues on multiple proteins including several of potential relevance to radiation protection. Specifically, binding of CDDO to Cys179 in IKKβ leads to inhibition of canonical NF-κB signaling (16) and binding to KEAP1 leads to increased levels of the transcription factor Nrf2 and of multiple antioxidant and phase-2 defense enzymes (17). RTA 408 was included in the screen because we previously observed robust radioprotection of zebrafish embryos by another variant of CDDO (CDDO-TFEA) (6). SB415286 and SB216763 are ATP competitive GSK3 inhibitors (18) whereas LiCl increases inhibitory phosphorylation of GSK3 (19). To allow direct side-by-side comparison all drugs were given using a standardized regimen, i.e. for 1 day and 1 h prior to radiation and daily for three days after. Drug dosages were guided by published results and administration was by intraperitoneal injection. We observed various levels of radiation protection with each of the compounds tested. The CDDO derivative RTA 408 provided robust and consistent levels of radiation protection (100% at 30 days post IR (8 Gy)) either as a single compound (Figure 1a) or in combination with the GSK3 inhibitor SB216763 (Figure 1c). In agreement with an earlier report (13), ethyl pyruvate also markedly increased survival of lethally irradiated mice (Figure 1a). Interestingly, the survival advantage provided by RTA 408 was compromised when combined with SB415286 but not when combined with SB216763 (Figure 1c). Similarly, survival of lethally irradiated mice treated with a combination of RTA 408 and LiCl was slightly lower than survival of mice receiving RTA 408 alone (Figure 1c). Finally, RTA 408 produced levels of radiation protection similar to amifostine, the only currently approved radiation protector (Fig. 1d). These results encouraged us to further investigate tissue protection provided by RTA 408 alone.

RTA 408 protects mice against gastrointestinal syndrome and death after lethal doses of radiation

Next, we investigated the effect of RTA 408 on the small intestine in C57Bl/6 mice irradiated at a dose (9 Gy) that causes death from gastrointestinal syndrome within 10–15

days (20). We observed that RTA 408 preserved the integrity of the mucosal lining of the small intestine of lethally irradiated mice (Figure 2a). Mice that did not succumb to gastrointestinal syndrome lived beyond 30 days after IR, consistent with radiation protection of multiple organs including the hemopoietic system. Furthermore, as determined by Ki-67 staining RTA 408-treated mice revealed robust proliferation in the crypt area at 2 and 7 days after IR whereas radiation alone (9 Gy) markedly reduced proliferation in this tissue compartment concurrent with extensive tissue destruction (Figure 2a). RTA 408 also significantly reduced radiation-induced apoptosis in both, villi and crypts as determined by TUNEL staining (Figure 2b). This effect extended to the skin, in which RTA 408 similarly reduced the apoptosis incidence caused by radiation exposure (Supplementary Figure S1).

RTA 408 inhibits cell growth and survival of human prostate cancer in vivo

To address whether the cytoprotective effects of RTA 408 extended to tumor cells, we first tested the effects of RTA 408 on four different prostate cancer cell lines representing advanced, androgen-independent tumor stages (LNCaP/C4-2B, CWR22Rv1, DU145 and PC3). We observed robust tumor growth inhibition by RTA 408 of established xenografts (tumor size > 30 mm^3 when treatment commenced) of all four cell lines tested even in the absence of radiation. Tumor growth, as determined by caliper measurements, is shown in Figure 3a and representative in vivo tumor images at different days post-treatment in Supplementary Figure S2. In marked contrast to the protective effects observed in normal tissues, RTA 408 did not radioprotect PC3 xenotransplants. Rather, when used in combination with radiation, RTA 408 amplified the anti-tumor effect of radiation alone ($p=0.001$) (Figure 3b). In vivo imaging revealed complete tumor growth inhibition in animals that received both radiation and RTA 408 at 17.5 mg/kg (see insert, Figure 3b) but not in mice treated with 5 mg/kg RTA 408 (not shown). RTA 408 induced high levels of intratumoral apoptosis as determined by detection of fragmented DNA (TUNEL), cleaved PARP, and the caspase3 cleavage product of cytokeratin18 (Figure 4a). The antibodies used to detect cleaved PARP and cytokeratin18 do not crossreact with mouse tissues indicating that RTA 408 induced apoptosis of human tumor cells in situ. RTA 408-dependent inhibition of PC3 xenografts was associated with significantly reduced proliferation as determined by Ki-67 staining (Figure 4b).

RTA 408 decreases growth and survival of human prostate cancer cells in vitro

Next, we examined dose-dependent effects of RTA 408 on prostate cancer cells in vitro. Within 24 h of exposure, RTA 408 (1 μM) induced varying degrees of apoptosis in all four prostate cancer cell lines as determined by detection of cleaved caspase3, cytokeratin18, and PARP-1 in both attached and, more prominently, in cells detached from substrate (Supplementary Figure S3). By contrast, caspase 8 cleavage was only marginally detected in DU145 at the higher doses of RTA 408 (0.5–1 μM) tested but not the other three cell lines. As determined by clonogenic survival assays, RTA 408 radiosensitized all four prostate cancer cell lines under investigation with the strongest effects observed in DU145 and LNCaP/C4-2B cells (Supplementary Figure S4). As assessed by crystal violet staining and by WST assay, RTA 408 reduced viability of all four prostate cancer cell lines in a dose-dependent fashion (Figure 5a). The IC_{50} for inhibition of in vitro growth and survival of these cell lines ranged from 250 to 750 nM. Interestingly, RTA 408 also inhibited in vitro

growth and survival of normal primary prostate epithelial cells (PrEC), the immortalized NHPr-E1 and BHPrE-1 prostate cells and, primary human epidermal keratinocytes (NHEK-1, -2, and -3) (Figure 5b). The IC_{50} as determined by crystal violet staining for the normal or premalignant cells was in the range of 125 to 250 nM. Compromised cell viability was associated with substrate detachment of normal prostate epithelial cells and keratinocytes, as well as control PC3 cells (Supplementary Figure S5). Collectively, these results highlight a broad spectrum of inhibitory effects of RTA 408 on benign and malignant prostate cells and on normal prostate epithelial cells and keratinocytes in vitro. The effects on normal epithelial cells in vitro are in marked contrast to tissue protection of normal epithelial tissues in irradiated mice.

Inhibition of NF-κB activity by RTA 408 in vivo

The selective anti-tumor activity of RTA 408 on prostate cancer cell lines in vivo raises the question which molecular target(s) are responsible for this effect. In prostate cancer, deregulated NF-κB signaling is associated with disease progression, contributes to expression of both prostate specific antigen (PSA) (21) and androgen receptor (22), and is prevalent in castrate-resistant and metastatic tumors (23–26). Conversely, disrupting NF-κB signaling by forced expression of a phosphorylation-deficient IκB radiosensitizes PC3 prostate cells in vitro (27). Other NF-κB inhibitors including curcumin (28), parthenolide (29), and SN52 (30) similarly inhibit prostate cancer growth and survival. Based on this prior work, we used NF-κB-NLuc- and control CMV-Fluc -reporter constructs to measure NF-κB activity in transfected PC3 tumors in vivo, before and after treatment with RTA 408 and/or IR (Figure 6a,b). As expected, radiation induced NF-κB activity in tumor tissue (Figure 6, panel 4). In the post-treatment group the ratio of NF-κB-NLuc- to CMV-Fluc activity in RTA 408 treated mice (Figure 6, panel 6) was significantly lower compared to that observed in mice treated with vehicle alone (Figure 6, panel 2). In addition, the ratio of NF-κB-NLuc- to CMV-Fluc activity in mice treated with RTA 408 and IR combined (Figure 6, panel 8) was significantly lower compared to that observed in mice treated with IR alone (Figure 6, panel 4). Hence, at tumor growth-inhibitory concentrations RTA 408 effectively inhibited transcription of an NF-κB-responsive reporter construct in PC3 cells in vivo.

These observations extend and confirm previous reports describing in vitro growth inhibition of human prostate cancer cells by CDDO variants. Specifically, Deeb et al. described proapoptotic effects of CDDO, CDDO-methyl(ME) and, CDDO-imidazole(IM) in cultured human LNCaP, PC3 and DU145 and murine TRAMPC-1 prostate cancer cells in vitro (31, 32). Furthermore, Gao et al. described CDDO-dependent chemoprevention of prostate cancer development in transgenic TRAMP mice in which the SV40 T antigen is expressed by prostate epithelial cells (33). Tumor growth inhibition by CDDO derivatives extends to other tumor types ranging from leukemias (34–37) to solid malignancies (38–42). A common denominator of these tumor types is deregulated NF-κB activity which is effectively inhibited by RTA 408 not only in vitro but also in vivo. It remains to be determined whether inhibition of survival pathways beyond NF-κB play a role in prostate cancer inhibition by RTA 408. For example, the Akt/mTOR pathway is also reportedly inhibited by CDDO-ME in prostate cancer cells (43).

The mechanistic basis for the dual and opposite effects of RTA 408 on normal and a broad range of malignant tissues remains to be investigated further. Of particular relevance to cytoprotection, CDDO covalently attaches to KEAP1, disrupts KEAP1/Nrf2 interaction and triggers Nrf2-dependent transcription of a host of genes encoding antioxidant enzymes (16). Nrf-2 activation by the CDDO derivatives CDDO-ethylamide (EA) and CDDO-ME has been proposed to improve survival of irradiated mice (44). We observed that topical application of RTA 408 markedly reduced radiation dermatitis in mice associated with significant increases in Nrf2 target genes and significant decreases in NF-kB target genes (45). Interestingly, radiation protection of normal prostate epithelial cells contrasted by growth inhibition of prostate cancer cells in vivo has been very recently described for dimethylamineparthenolide (DMAPT) (46). DMAPT and its parent compound parthenolide alkylate reactive cysteines on multiple protein targets including KEAP1 and inhibit canonical NF-κB signaling by interacting with IκB and the NFκBp65 subunit (47–49). In contrast to RTA 408, parthenolide or DMAPT reportedly did not inhibit cultured normal or immortalized prostate cells to the same extent as their malignant counterparts and this difference has been attributed to differential effects of DMAPT on KEAP1-dependent oxidation status in normal and malignant cells (46). This difference between RTA 408 and DMAPT suggests that tissue protection by RTA 408 as seen in vivo is not primarily due to cell-autonomous effects but likely depends on environmental factors provided by the tissue context in vivo. A precedent for ‘contextual’ anti-tumor effects of CDDO-ME has been established previously (50). Specifically, CDDO-ME inhibited myeloid-derived suppressor cells in the tumor micorenvironment associated with improved immune responses. Regardless of the relative contribution of cell-intrinsic or ‘environmental’ anti-tumor mechanisms, the results obtained for DMAPT (46) and RTA 408 (this study) validate the concept of selective radiosensitization of tumor cell tissues by thiol reactive compounds (5).

Supplementary Material

Refer to Web version on PubMed Central for supplementary material.

Acknowledgments

We thank Phyllis Wachsberger (Thomas Jefferson University) for advice on performing clonogenic assays, Simon Hayward (Vanderbilt University) for providing immortalized prostate cells and Marja Nevalainen (Thomas Jefferson University) for providing prostate cancer cells.

Grant support

This work was supported by DoD grant W81XWH-12-1-0477, and a pilot project under National Institute of Health grant U19A1091175. Additional support was provided by the Prostate Cancer Foundation and by REATA Pharmaceuticals.

References

1. Kountouras J, Zavos C. Recent advances in the management of radiation colitis. World J Gastroenterol. 2008; 14:7289–7301. [PubMed: 19109862]
2. Souhami L, Bae K, Pilepich M, Sandler H. Impact of the duration of adjuvant hormonal therapy in patients with locally advanced prostate cancer treated with radiotherapy: a secondary analysis of RTOG 85-31. J Clin Oncol. 2009; 27:2137–2143. [PubMed: 19307511]

3. Simone NL, Menard C, Soule BP, Albert PS, Guion P, Smith S, et al. Intrarectal amifostine during external beam radiation therapy for prostate cancer produces significant improvements in Quality of Life measured by EPIC score. Int J Radiat Oncol Biol Phys. 2008; 70:90–95. [PubMed: 17855015]

4. Spitz DRD, Hauer-Jensen M. Ionizing Radiation-Induced Responses: Where Free Radical Chemistry Meets Redox Biology and Medicine. Antioxid Redox Signal. 2013

5. Deorukhkar A, Krishnan S. Targeting inflammatory pathways for tumor radiosensitization. Biochem Pharmacol. 2010; 80:1904–1914. [PubMed: 20599771]

6. Daroczi B, Kari G, Ren Q, Dicker AP, Rodeck U. Nuclear factor kappaB inhibitors alleviate and the proteasome inhibitor PS-341 exacerbates radiation toxicity in zebrafish embryos. Mol Cancer Ther. 2009; 8:2625–2634. 4(3):427–34. [PubMed: 19723885]

7. Thotala DK, Hallahan DE, Yazlovitskaya EM. Inhibition of glycogen synthase kinase 3 beta attenuates neurocognitive dysfunction resulting from cranial irradiation. Cancer Res. 2008; 68:5859–5868. 64(7):2382–9. [PubMed: 18632640]

8. Thotala DK, Geng L, Dickey AK, Hallahan DE, Yazlovitskaya EM. A new class of molecular targeted radioprotectors: GSK-3beta inhibitors. Int J Radiat Oncol Biol Phys. 2010; 76:557–565. [PubMed: 20117291]

9. Jacobs KM, Bhave SR, Ferraro DJ, Jaboin JJ, Hallahan DE, Thotala D. GSK-3beta: A Bifunctional Role in Cell Death Pathways. International journal of cell biology. 2012; 2012:930710. [PubMed: 22675363]

10. Hoeflich KP, Luo J, Rubie EA, Tsao MS, Jin O, Woodgett JR. Requirement for glycogen synthase kinase-3beta in cell survival and NF-kappaB activation. Nature. 2000; 406:86–90. [PubMed: 10894547]

11. Cremer TJ, Shah P, Cormet-Boyaka E, Valvano MA, Butchar JP, Tridandapani S. Akt-mediated proinflammatory response of mononuclear phagocytes infected with Burkholderia cenocepacia occurs by a novel GSK3beta-dependent, IkappaB kinase-independent mechanism. J Immunol. 2011; 187:635–643. [PubMed: 21697459]

12. Hall, EJ.; Giaccia, AJ. Radiobiology for the radiologist. Philadelphia: Lippincott Williams & Wilkins; 2006. Cell survival curves; p. 30-46.

13. Epperly M, Jin S, Nie S, Cao S, Zhang X, Franicola D, et al. Ethyl pyruvate, a potentially effective mitigator of damage after total-body irradiation. Radiat Res. 2007; 168:552–559. [PubMed: 17973549]

14. Daroczi B, Kari G, McAleer MF, Wolf JC, Rodeck U, Dicker AP. In vivo radioprotection by the fullerene nanoparticle DF-1 as assessed in a zebrafish model. Clin Cancer Res. 2006; 12:7086–7091. 12(1):20–8. [PubMed: 17145832]

15. Han Y, Englert JA, Yang R, Delude RL, Fink MP. Ethyl pyruvate inhibits nuclear factor-kappaB-dependent signaling by directly targeting p65. J Pharmacol Exp Ther. 2005; 312:1097–1105. [PubMed: 15525791]

16. Ahmad R, Raina D, Meyer C, Kharbanda S, Kufe D. Triterpenoid CDDO-Me blocks the NF-kappaB pathway by direct inhibition of IKKbeta on Cys-179. Journal of Biological Chemistry. 2006; 281:35764–35769. [PubMed: 16998237]

17. Liby K, Hock T, Yore MM, Suh N, Place AE, Risingsong R, et al. The synthetic triterpenoids, CDDO and CDDO-imidazolide, are potent inducers of heme oxygenase-1 and Nrf2/ARE signaling. Cancer Res. 2005; 65:4789–4798. 64(7):2382–9. [PubMed: 15930299]

18. Coghlan MP, Culbert AA, Cross DA, Corcoran SL, Yates JW, Pearce NJ, et al. Selective small molecule inhibitors of glycogen synthase kinase-3 modulate glycogen metabolism and gene transcription. Chem Biol. 2000; 7:793–803. [PubMed: 11033082]

19. Zhang F, Phiel CJ, Spece L, Gurvich N, Klein PS. Inhibitory phosphorylation of glycogen synthase kinase-3 (GSK-3) in response to lithium. Evidence for autoregulation of GSK-3. J Biol Chem. 2003; 278:33067–33077. [PubMed: 12796505]

20. Saha S, Bhanja P, Liu L, Alfieri AA, Yu D, Kandimalla ER, et al. TLR9 agonist protects mice from radiation-induced gastrointestinal syndrome. PLoS One. 2012; 7:e29357. [PubMed: 22238604]

21. Chen CD, Sawyers CL. NF-kappa B activates prostate-specific antigen expression and is upregulated in androgen-independent prostate cancer. Mol Cell Biol. 2002; 22:2862–2870. [PubMed: 11909978]
22. Zhang L, Altuwaijri S, Deng F, Chen L, Lal P, Bhanot UK, et al. NF-kappaB regulates androgen receptor expression and prostate cancer growth. Am J Pathol. 2009; 175:489–499. [PubMed: 19628766]
23. McCall P, Bennett L, Ahmad I, Mackenzie LM, Forbes IW, Leung HY, et al. NFkappaB signalling is upregulated in a subset of castrate-resistant prostate cancer patients and correlates with disease progression. Br J Cancer. 2012; 107:1554–1563. [PubMed: 23093296]
24. Siddiqui IA, Shukla Y, Adhami VM, Sarfaraz S, Asim M, Hafeez BB, et al. Suppression of NFkappaB and its regulated gene products by oral administration of green tea polyphenols in an autochthonous mouse prostate cancer model. Pharmaceutical research. 2008; 25:2135–2142. [PubMed: 18317887]
25. Andela VB, Gordon AH, Zotalis G, Rosier RN, Goater JJ, Lewis GD, et al. NFkappaB: a pivotal transcription factor in prostate cancer metastasis to bone. Clin Orthop Relat Res. 2003:S75–S85. [PubMed: 14600595]
26. Jin R, Sterling JA, Edwards JR, DeGraff DJ, Lee C, Park SI, et al. Activation of NF-kappa B signaling promotes growth of prostate cancer cells in bone. PLoS One. 2013; 8:e60983. [PubMed: 23577181]
27. Pajonk F, Pajonk K, McBride WH. Inhibition of NF-kappaB, clonogenicity, and radiosensitivity of human cancer cells. J Natl Cancer Inst. 1999; 91:1956–1960. [PubMed: 10564680]
28. Chendil D, Ranga RS, Meigooni D, Sathishkumar S, Ahmed MM. Curcumin confers radiosensitizing effect in prostate cancer cell line PC-3. Oncogene. 2004; 23:1599–1607. [PubMed: 14985701]
29. Sun Y, St Clair DK, Fang F, Warren GW, Rangnekar VM, Crooks PA, et al. The radiosensitization effect of parthenolide in prostate cancer cells is mediated by nuclear factor-kappaB inhibition and enhanced by the presence of PTEN. Mol Cancer Ther. 2007; 6:2477–2486. 4(3):427–34. [PubMed: 17876045]
30. Xu Y, Fang F, St Clair DK, Sompol P, Josson S, St Clair WH. SN52, a novel nuclear factor-kappaB inhibitor, blocks nuclear import of RelB:p52 dimer and sensitizes prostate cancer cells to ionizing radiation. Mol Cancer Ther. 2008; 7:2367–2376. 4(3):427–34. [PubMed: 18723484]
31. Deeb D, Gao X, Dulchavsky SA, Gautam SC. CDDO-me induces apoptosis and inhibits Akt, mTOR and NF-kappaB signaling proteins in prostate cancer cells. Anticancer research. 2007; 27:3035–3044. [PubMed: 17970042]
32. Deeb D, Gao X, Dulchavsky SA, Gautam SC. CDDO-Me inhibits proliferation, induces apoptosis, down-regulates Akt, mTOR, NF-kappaB and NF-kappaB-regulated antiapoptotic and proangiogenic proteins in TRAMP prostate cancer cells. J Exp Ther Oncol. 2008; 7:31–39. [PubMed: 18472640]
33. Gao X, Deeb D, Liu Y, Arbab AS, Divine GW, Dulchavsky SA, et al. Prevention of Prostate Cancer with Oleanane Synthetic Triterpenoid CDDO-Me in the TRAMP Mouse Model of Prostate Cancer. Cancers (Basel). 2011; 3:3353–3369. [PubMed: 21961053]
34. Shishodia S, Sethi G, Konopleva M, Andreeff M, Aggarwal BB. A synthetic triterpenoid, CDDO-Me, inhibits IkappaBalpha kinase and enhances apoptosis induced by TNF and chemotherapeutic agents through down-regulation of expression of nuclear factor kappaB-regulated gene products in human leukemic cells. Clin Cancer Res. 2006; 12:1828–1838. 12(1):20–8. [PubMed: 16551868]
35. Samudio I, Kurinna S, Ruvolo P, Korchin B, Kantarjian H, Beran M, et al. Inhibition of mitochondrial metabolism by methyl-2-cyano-3,12-dioxooleana-1,9-diene-28-oate induces apoptotic or autophagic cell death in chronic myeloid leukemia cells. Mol Cancer Ther. 2008; 7:1130–1139. [PubMed: 18483301]
36. Stadheim TA, Suh N, Ganju N, Sporn MB, Eastman A. The novel triterpenoid 2-cyano-3,12-dioxooleana-1,9-dien-28-oic acid (CDDO) potently enhances apoptosis induced by tumor necrosis factor in human leukemia cells. The Journal of biological chemistry. 2002; 277:16448–16455. [PubMed: 11880365]

37. Pedersen IM, Kitada S, Schimmer A, Kim Y, Zapata JM, Charboneau L, et al. The triterpenoid CDDO induces apoptosis in refractory CLL B cells. Blood. 2002; 100:2965–2972. 94(8):2562–8. [PubMed: 12351409]
38. Qin Y, Deng W, Ekmekcioglu S, Grimm EA. Identification of unique sensitizing targets for anti-inflammatory CDDO-Me in metastatic melanoma by a large-scale synthetic lethal RNAi screening. Pigment Cell Melanoma Res. 2013; 26:97–112. [PubMed: 23020131]
39. Konopleva M, Zhang W, Shi YX, McQueen T, Tsao T, Abdelrahim M, et al. Synthetic triterpenoid 2-cyano-3,12-dioxooleana-1,9-dien-28-oic acid induces growth arrest in HER2-overexpressing breast cancer cells. Mol Cancer Ther. 2006; 5:317–328. [PubMed: 16505105]
40. Duan Z, Ames RY, Ryan M, Hornicek FJ, Mankin H, Seiden MV. CDDO-Me, a synthetic triterpenoid, inhibits expression of IL-6 and Stat3 phosphorylation in multi-drug resistant ovarian cancer cells. Cancer chemotherapy and pharmacology. 2009; 63:681–689. [PubMed: 18587580]
41. Gao X, Deeb D, Liu P, Liu Y, Arbab-Ali S, Dulchavsky SA, et al. Role of reactive oxygen species (ROS) in CDDO-Me-mediated growth inhibition and apoptosis in colorectal cancer cells. J Exp Ther Oncol. 2011; 9:119–127. [PubMed: 21699019]
42. Zou W, Chen S, Liu X, Yue P, Sporn MB, Khuri FR, et al. c-FLIP downregulation contributes to apoptosis induction by the novel synthetic triterpenoid methyl-2-cyano-3, 12-dioxooleana-1, 9-dien-28-oate (CDDO-Me) in human lung cancer cells. Cancer biology & therapy. 2007; 6:1614–1620. [PubMed: 18253090]
43. Deeb D, Gao X, Jiang H, Janic B, Arbab AS, Rojanasakul Y, et al. Oleanane triterpenoid CDDO-Me inhibits growth and induces apoptosis in prostate cancer cells through a ROS-dependent mechanism. Biochemical Pharmacology. 2010; 79:350–360. [PubMed: 19782051]
44. Kim SB, Pandita RK, Eskiocak U, Ly P, Kaisani A, Kumar R, et al. Targeting of Nrf2 induces DNA damage signaling and protects colonic epithelial cells from ionizing radiation. Proc Natl Acad Sci U S A. 2012; 109:E2949–E2955. 102(6):1915–20. [PubMed: 23045680]
45. Reisman SA, Lee C-Y, Meyer CJ, Proksch JW, Sonis ST, Ward KW. Topical application of the synthetic triterpenoid RTA 408 protects mice from radiation-induced dermatitis. Radiat Res. 2014 in press.
46. Xu Y, Fang F, Miriyala S, Crooks PA, Oberley TD, Chaiswing L, et al. KEAP1 Is a Redox Sensitive Target That Arbitrates the Opposing Radiosensitive Effects of Parthenolide in Normal and Cancer Cells. Cancer Res. 2013; 73:4406–4417. [PubMed: 23674500]
47. Garcia-Pineres AJ, Castro V, Mora G, Schmidt TJ, Strunck E, Pahl HL, et al. Cysteine 38 in p65/NF-kappaB plays a crucial role in DNA binding inhibition by sesquiterpene lactones. J Biol Chem. 2001; 276:39713–39720. [PubMed: 11500489]
48. Kwok BH, Koh B, Ndubuisi MI, Elofsson M, Crews CM. The anti-inflammatory natural product parthenolide from the medicinal herb Feverfew directly binds to and inhibits IkappaB kinase. Chem Biol. 2001; 8:759–766. [PubMed: 11514225]
49. Hehner SP, Hofmann TG, Droge W, Schmitz ML. The antiinflammatory sesquiterpene lactone parthenolide inhibits NF-kappa B by targeting the I kappa B kinase complex. J Immunol. 1999; 163:5617–5623. [PubMed: 10553091]
50. Nagaraj S, Youn JI, Weber H, Iclozan C, Lu L, Cotter MJ, et al. Anti-inflammatory triterpenoid blocks immune suppressive function of MDSCs and improves immune response in cancer. Clin Cancer Res. 2010; 16:1812–1823. [PubMed: 20215551]

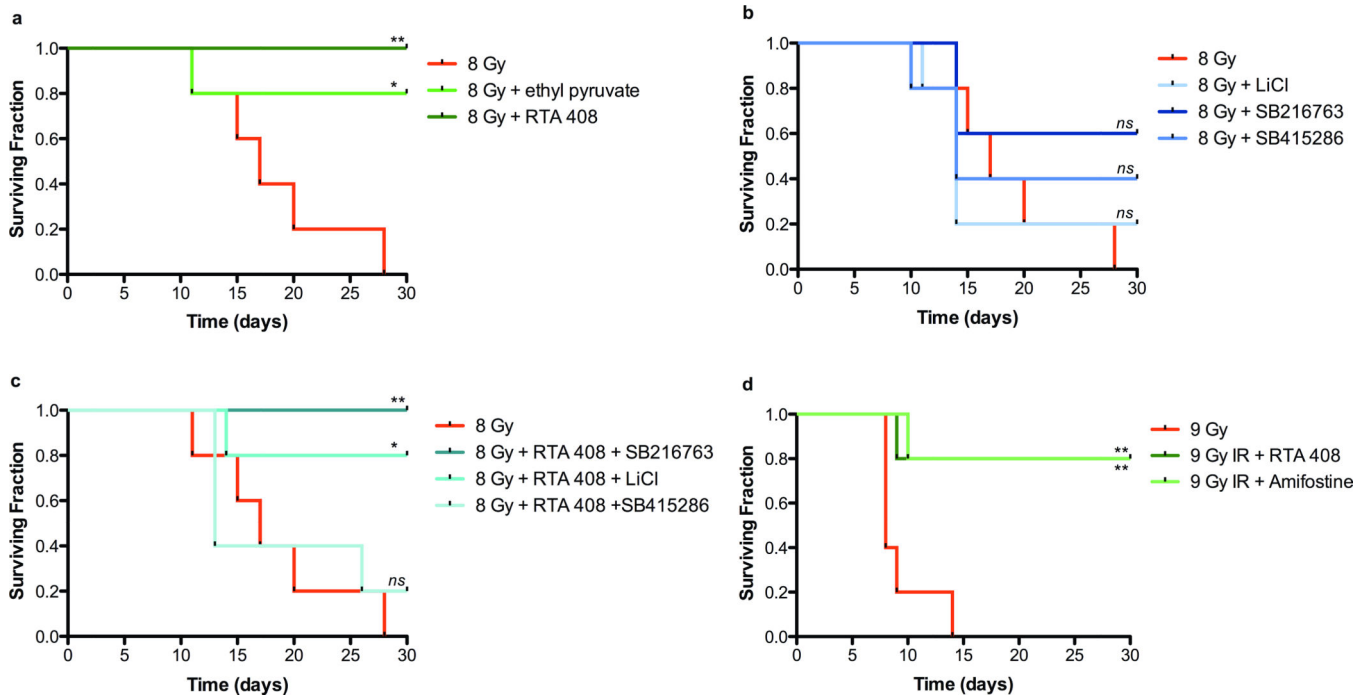

Figure 1.

Effects of signal transduction modifiers on survival of lethally irradiated mice. (a) Survival of mice pretreated (24 h) with the NF-κB inhibitors ethyl pyruvate (EP; 70 mg/kg) or RTA 408 (17.5 mg/kg) and receiving 8 Gy single dose whole body radiation. Ethyl pyruvate was administered 15 min prior to IR and on days 1 – 3 post IR. RTA 408 was administered 1 d and 1 h pre-irradiation and on days 1 – 3 post IR. (b) Survival of mice treated with the GSK3 inhibitors Lithium chloride (LiCl; 40 mg/kg), SB415286 (1 mg/kg) and SB216673 (1 mg/kg) and receiving 8 Gy single dose whole body radiation; treatment schedule for these compounds was 2 and 1 day prior to IR and daily on days 1 – 3 post IR. (c) Effects of select combinations of NF-κB and GSK3 inhibitors on survival of irradiated mice (8 Gy); treatment schedules for individual compounds as described under panel A. (d) Survival of irradiated mice (whole body, 9 Gy) treated with RTA 408 (17.5 mg/kg) at 24 and 1 h prior to IR and on days 1–2 post IR or with Amifostine (250 mg/kg) administered 15 min prior to IR. Experimental groups in each panel consisted of 5 animals each. P value summaries refer to pair-wise comparisons between IR and (IR + drug) treatment groups, generated by using the Log-rank (Mantel-Cox) test.

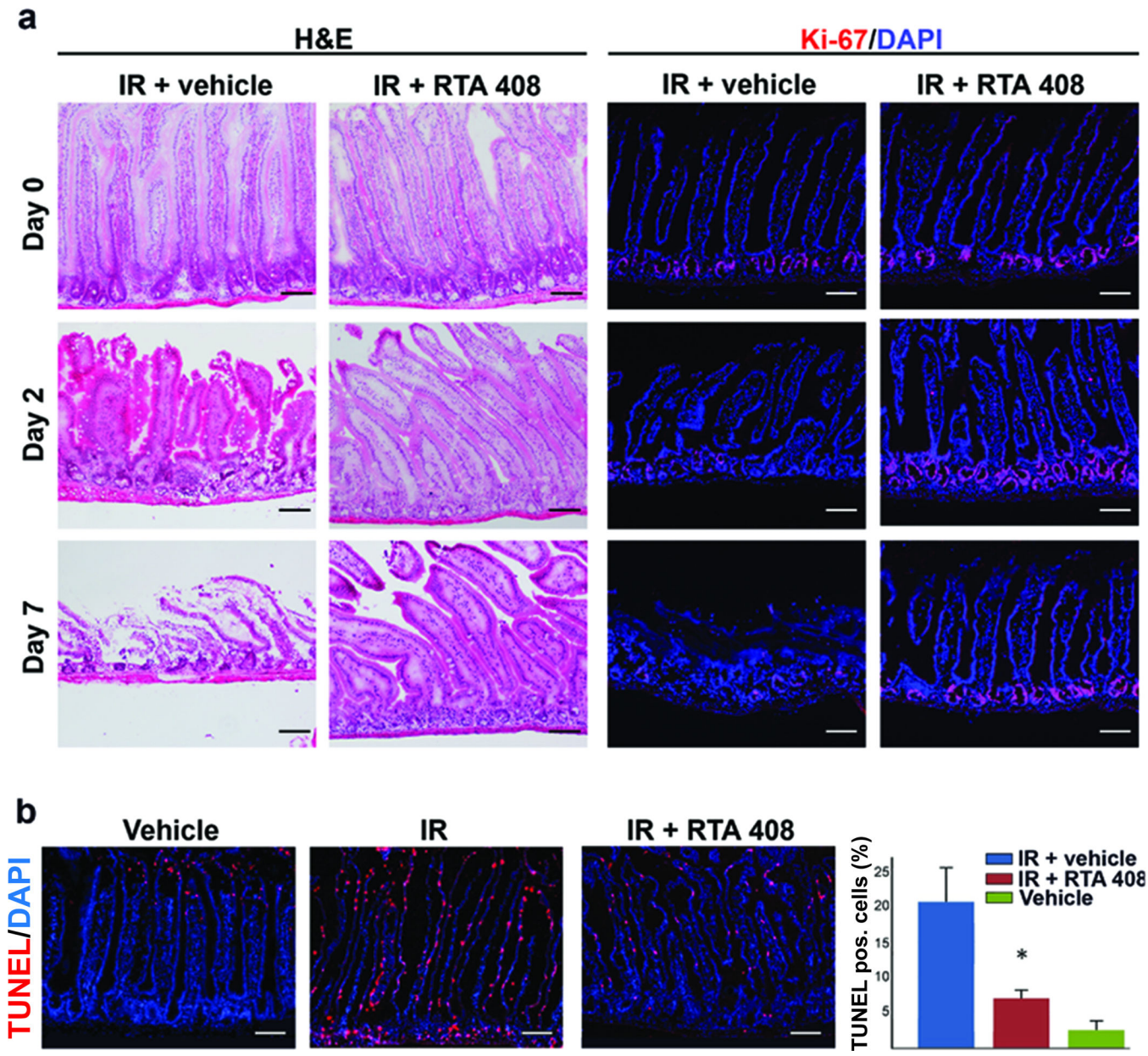

Figure 2.

RTA 408 reduces radiation-associated damage to the mucosal lining of the small intestine after single dose (9 Gy) radiation exposure. RTA 408 (17.5 mg/kg) was administered on days 1 – 3 post IR. (a) Assessment of gastrointestinal morphology was performed on tissue sections sampled days 2 and 7 after radiation exposure. Parallel sections were subjected to staining with Ki-67 reactive antibody to ascertain the proliferative state of the gastrointestinal stem cell compartment located in the crypt areas; scale bars = 100 μm. (b) Effects of RTA 408 on radiation-induced apoptosis incidence in the gastrointestinal mucosa. RTA 408 (17.5 mg/kg) was administered 24 h after IR (9 Gy) and small intestine tissues sampled at 48 h. Apoptosis incidence was determined by TUNEL staining and cell nuclei were counterstained with DAPI; scale bars = 100 μm. Results shown in panel D represent m

±SD of at least 6 fields/per condition analyzed. The number of TUNEL positive cells was significantly (Student's t-test ($p<0.05$)) reduced in irradiated animals receiving RTA 408 when compared to vehicle-treated, irradiated animals.

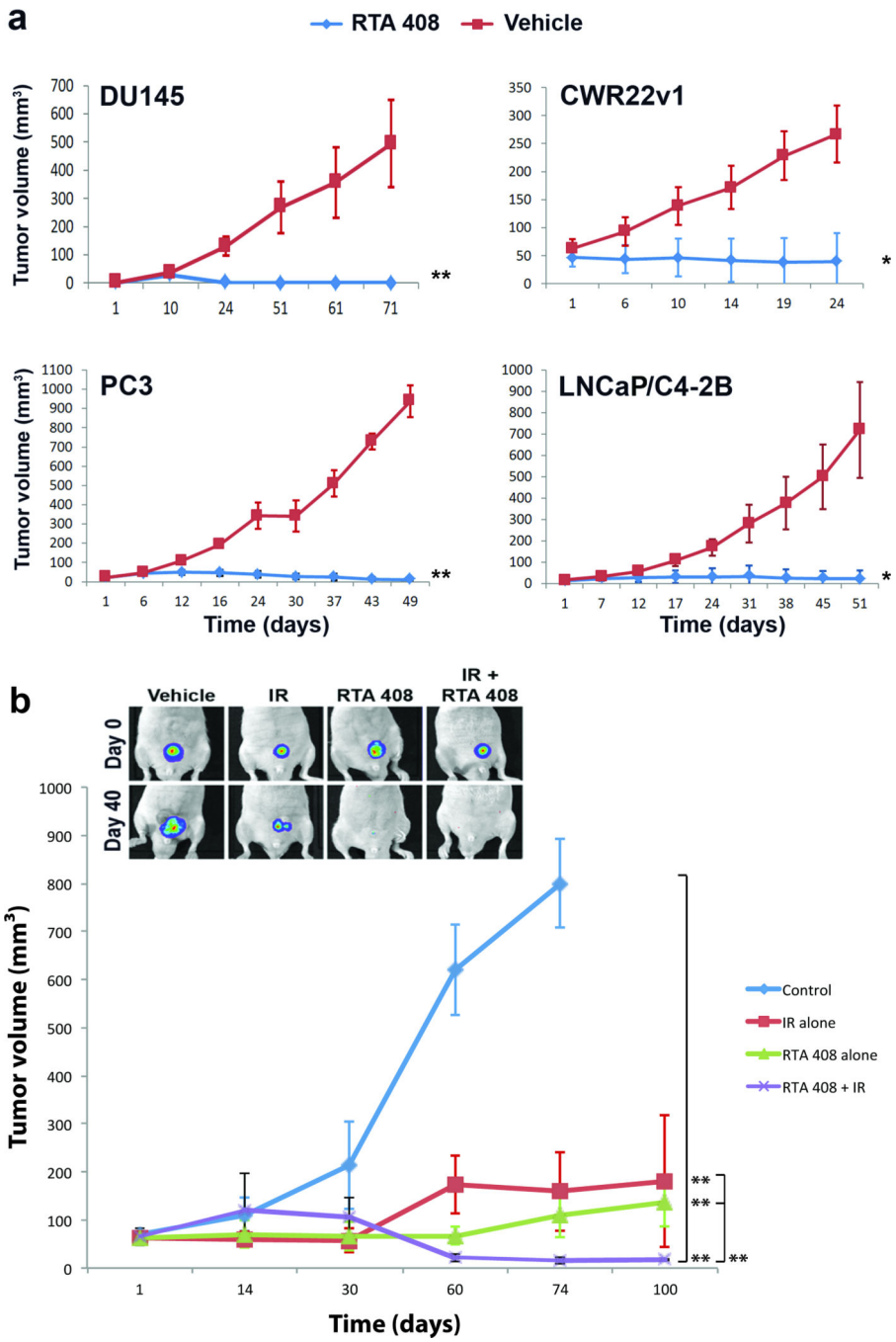

Figure 3.

RTA 408 inhibits growth and survival of human prostate cancer xenotransplants. (a) Effects of RTA 408 on growth of DU145, PC3, LNCaP/C4-2B and CWR22Rv1 cells in vivo. RTA 408 was administered (3× per week at 17.5 mg/kg) after tumors had reached volumes exceeding 25 – 30 mm^3. Experimental groups consisted of 5 animals each. Results represent m±SD of these groups. P value summaries refer to tumor growth trajectories over time in RTA 408 and control groups. (b) Inhibition of PC3 xenograft growth and survival by combined radiation and RTA 408 treatment. Tumor-bearing mice were treated for 2 weeks

with either RTA 408 or RTA 408 and IR. IR (5 Gy) was administered twice on days 1 and 8 and RTA 408 (17.5 mg/kg) was administered 1 d prior and for 3 days after each IR in the combination group. RTA 408 administration (3× weekly) was continued for further 4 weeks. Results represent m±SD of groups of 5 animals each. Tumor growth trajectories over time were compared between treatment and control groups, and among treatment groups. The insert shows representative images of tumors in situ at treatment start and 40 days after. Chemiluminescence was detected by IVIS bioimaging of PC3 cells constitutively expressing firefly luciferase.

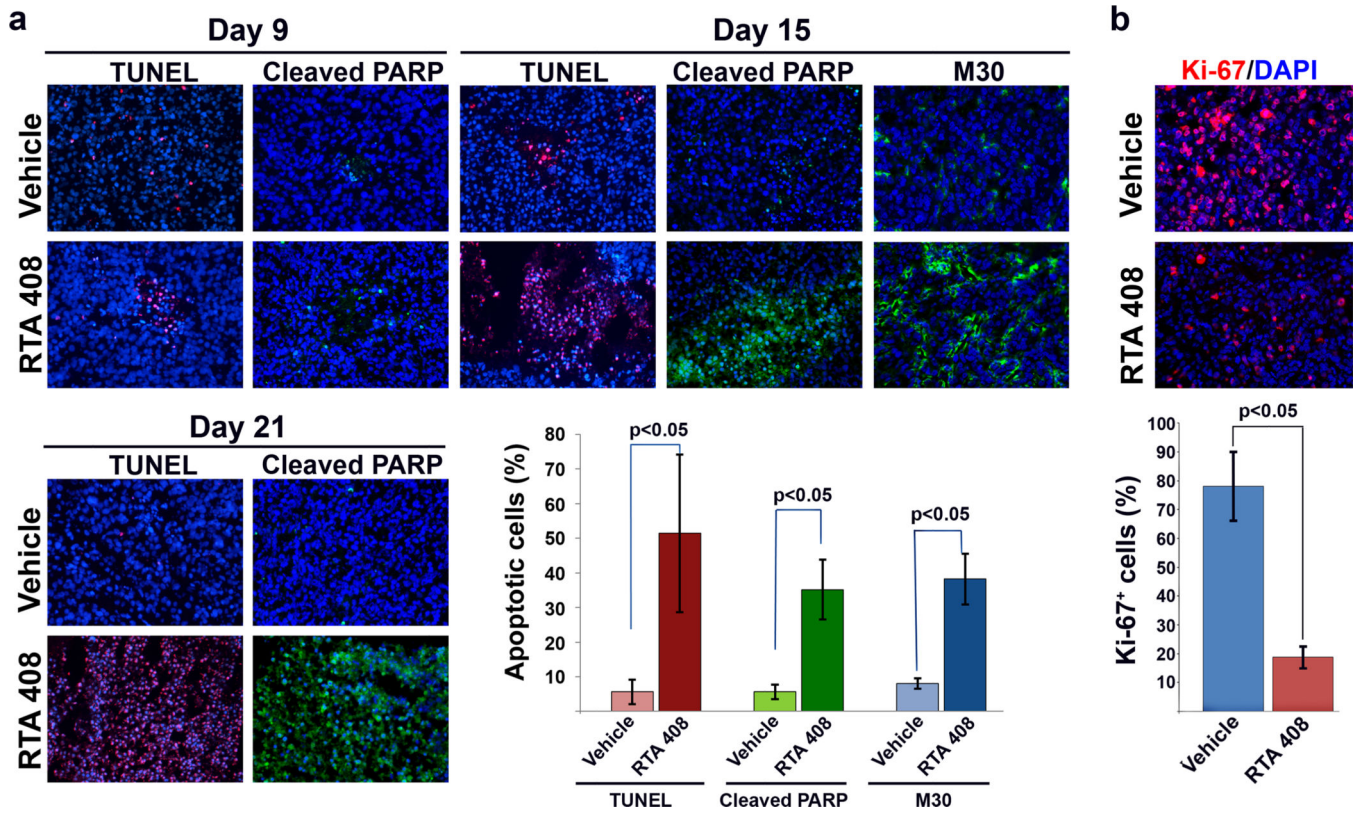

Figure 4.

Effects of RTA 408 on apoptosis incidence and proliferation in PC3 prostate cancer xenografts treated with RTA 408. (a) Apoptosis incidence was determined by TUNEL and by immunohistochemical detection of cleaved PARP and cytokeratin 18 (M30) at different time intervals after treatment with RTA 408 commenced; scale bars = 100 μm. Quantitative analysis of the results obtained on day 15 of treatment was performed by averaging the number of positive cells in at least 6 different fields. Results are expressed as m±SD. Statistically significant ($p<0.05$) differences were determined by Student's t-test. (b) RTA 408-dependent inhibition of PC3 prostate cancer cell proliferation. Proliferating cells were detected by staining with Ki-67 antibody (red). Cell nuclei were counterstained with DAPI; scale bars = 100 μm. Tumors were harvested 15 days after treatment initiation.

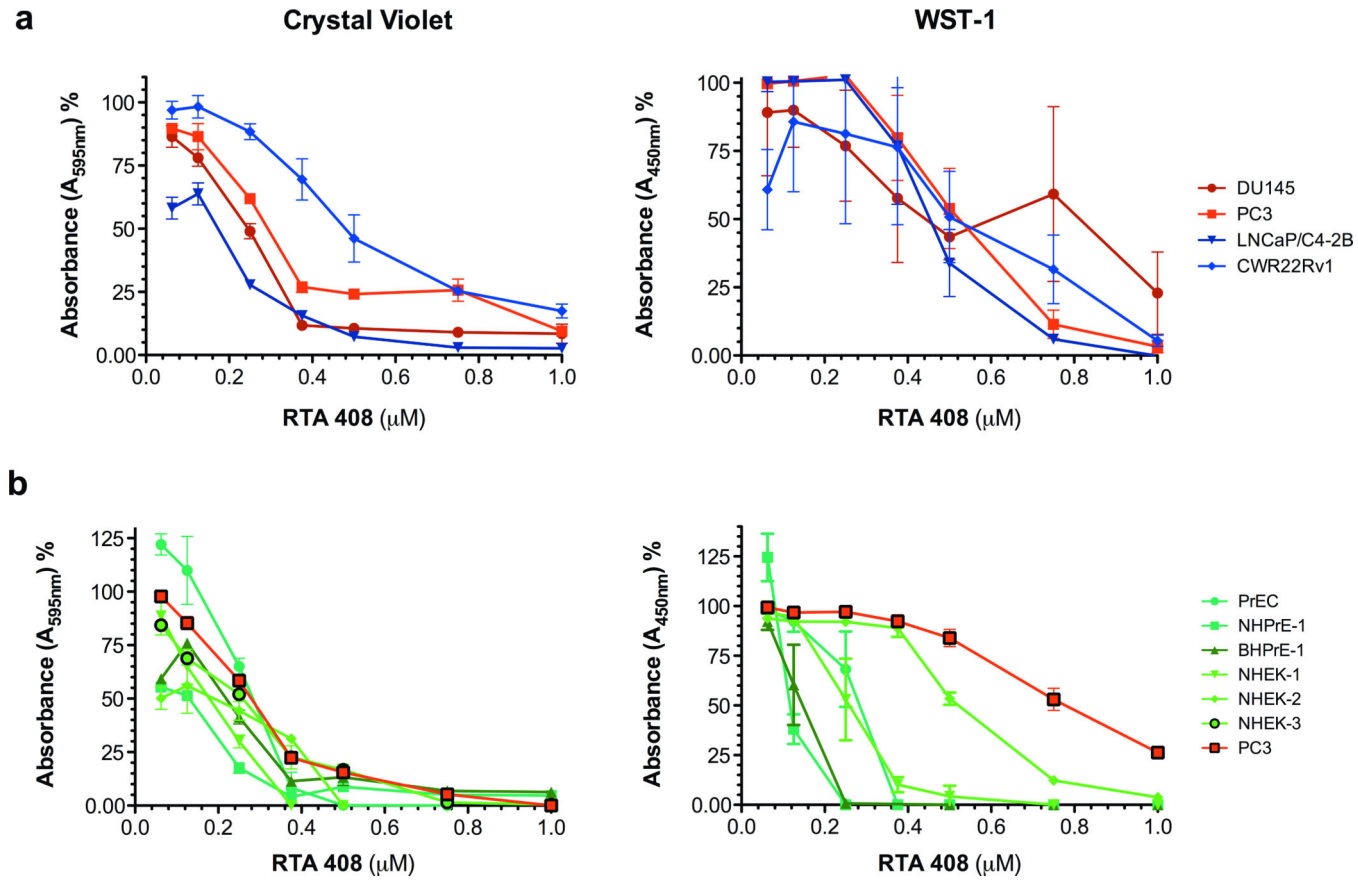

Figure 5.

In vitro effects of RTA 408 on (a) prostate cancer cell and (b) normal cell growth and survival. Loss of viability was determined by assessing the numbers of adherent cells using crystal violet stain or measuring metabolic activity (WST assay). Experiments were performed in triplicate and repeated 2 times. Results shown are m±SD of triplicates of a representative experiment. Results are presented as percentages of vehicle control. Analysis by using one-way ANOVA with Tukey's post-test correction (GraphPad Prism) revealed significant differences between RTA 408- and vehicle-treated groups ($p<0.05$ to $p<0.001$).

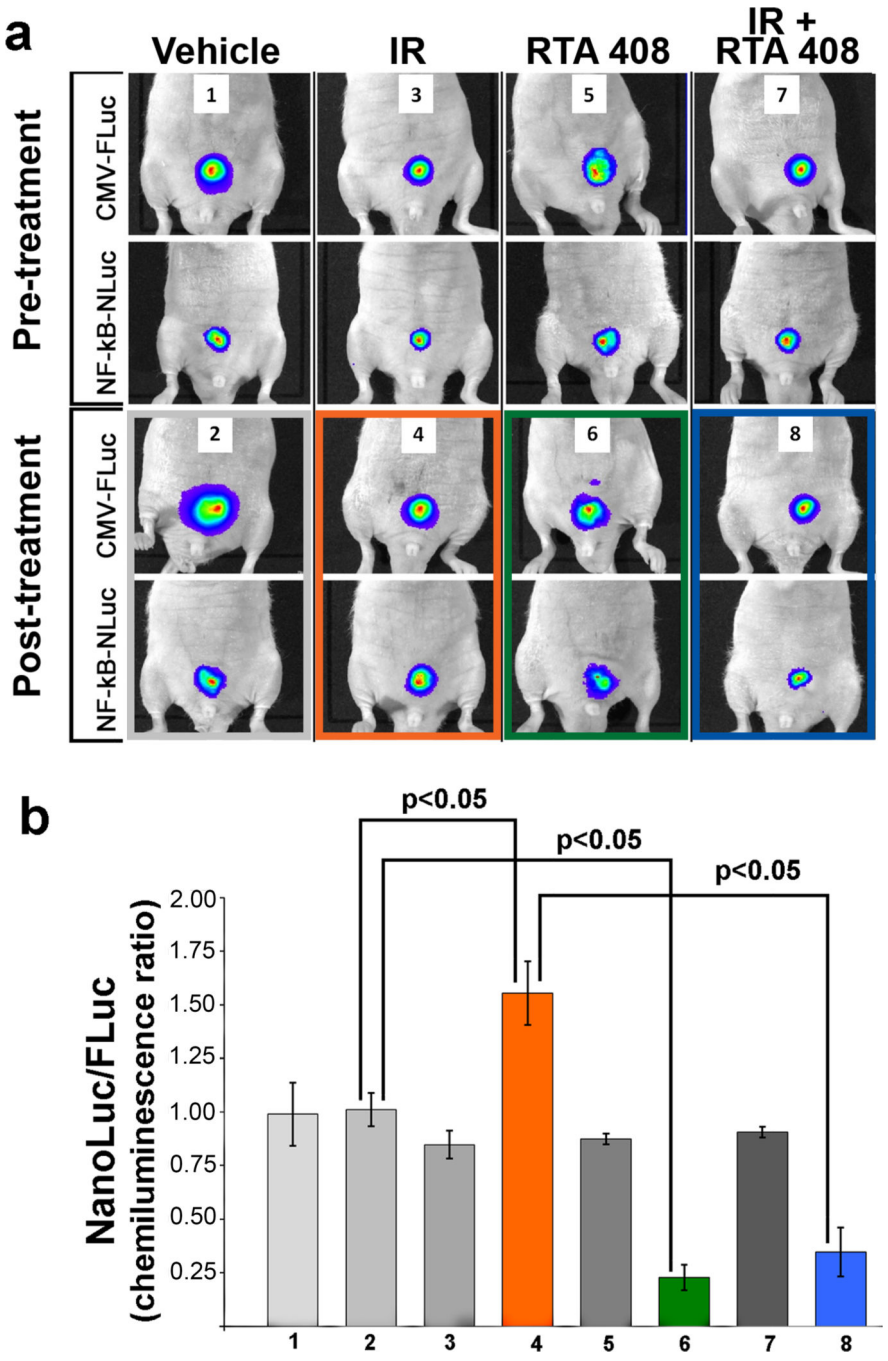

Figure 6.

In vivo imaging of NF-κB reporter activity in PC3 xenografts treated with either IR, or RTA 408 or a combination of IR and RTA 408. (a) Representative images of mice showing expression of firefly luciferase (Fluc) under control of a CMV promoter and corresponding images showing activity of an NF-κB responsive promoter driving NanoLuc® (NLuc) expression are shown. Pre-treatment images were acquired 2 days prior to treatment with either RTA 408 or IR (panels 1, 3, 5, 7). Post-treatment images were acquired from the same mice either untreated or after short-term (1 h) treatment with RTA 408 (17.5 mg/kg) or after

IR (5 Gy) or RTA 408 (17.5 mg/ml; 2 d) and IR (5 Gy) as indicated (panels 2,4,6,8). Images in the post-treatment group were acquired 1 h after IR exposure. (b) Quantitative representation of NF-κB 24 activity expressed as the ratio of NanoLuc® to firefly luciferase (n = 2 per group). Labeling of the X-axis refers to treatment groups as shown in panel (a). Results shown are m±SD of duplicate mice in each group. This experiment was repeated with comparable results.